Compact, simple and robust cross polarized wave generation source of few-cycle, high-contrast pulses for seeding petawatt-class laser systems

Patricia Ramirez, Dimitris N. Papadopoulos, Marc Hanna, Alain Pellegrina, Florence Friebel, Patrick Georges, Frédéric Druon

Compact, simple, and robust cross polarized wave generation source of few-cycle, high-contrast pulses for seeding petawatt-class laser systems

Lourdes Patricia Ramirez,[1,2,*] Dimitrios Papadopoulos,[1,2] Marc Hanna,[1] Alain Pellegrina,[2] Florence Friebel,[1] Patrick Georges,[1] and Frédéric Druon[1]

[1]*Laboratoire Charles Fabry, Institut d'Optique, CNRS, Univ. Paris Sud, 2, Avenue Augustin Fresnel, 91127 Palaiseau Cedex, France*

[2]*Laboratoire d'Utilisation des Lasers Intenses, Ecole Polytechnique, 91128 Palaiseau Cedex, France*

**Corresponding author: patricia.ramirez@institutoptique.fr*

A compact and robust, dual-crystal cross polarized wave generation setup combined with a hollow waveguide filter is implemented to deliver few-cycle, high-contrast laser pulses sourced from a commercial multipass Ti:Sa amplifier. The initial 25-fs pulses with a temporal contrast of 10^8 are shortened to 10 fs with an improved contrast of at least 10^{10}. The single nonlinear stage for spectral broadening and contrast enhancement of a commercial amplifier serves as an ideal injector for petawatt-class laser systems.

1. INTRODUCTION

Two crucial aspects in building a petawatt-class laser system is the pulse duration and the temporal contrast of the output laser pulses. Due to the limitation of crystal and grating sizes, ideally, shorter, few-cycle (5–10 fs) pulse durations are desired as less energy is required to achieve peak powers reaching the multipetawatt level. However, simultaneous amplification and bandwidth preservation of these ultrashort pulses is difficult with conventional laser amplifiers based on titanium-doped sapphire (Ti:Sa), which, as a result of gain narrowing, typically produce durations in the range of 20–25 fs. To circumvent this issue, several architectures for petawatt-class laser systems [1–3] involve optical parametric chirped pulse amplification (OPCPA) [4] which offers an advantage over conventional laser amplifiers in terms of bandwidth, since it supports the amplification of few-cycle pulses. On the other hand, the temporal contrast is the ratio of the peak intensity with respect to the parasitic structures such as prepulses and pedestals of the pulse in the picosecond (mainly coherent) and nanosecond (mainly incoherent) timescale. At the ultrahigh intensities achievable with petawatt-class lasers ($>10^{20}$ W/cm^2), these parasitic structures may reach a level that can preionize the target (10^{10} W/cm^2), leading to plasma preformation before the arrival of the main peak—an occurrence that directly alters the outcome of the experiment [5]. Therefore, temporal contrast enhancement must be implemented in any petawatt-class laser to keep the contrast ratio of the pulse below target preionization.

A high-fidelity, robust, and stable seed source is preferred for operational petawatt-class laser systems. Recently, few-cycle and high-contrast seed sources have been demonstrated via hollow fiber compression and cross-polarized generation (XPW) [6,7], a combination of hollow fiber compression, filamentation, and short-pulse OPCPA [8] and for slightly longer pulses at 15 fs, short-pulse OPCPA alone [9]. Hollow fiber compression [10] and filamentation [11] are self-phase modulation (SPM)-based techniques for spectral broadening which generate spectra supporting extremely short pulses (~5 fs) while cross polarized wave generation [12] and short pulse OPCPA [13] are temporal contrast enhancement techniques typically used at the front end of a laser chain. Despite the ultrabroad spectra obtainable via hollow fiber compression and filamentation, the stability and reproducibility of these spectra rely highly on the alignment of the hollow fiber and gas pressure [14], parameters which may change on a day-to-day basis and most importantly, during the operation of the laser system. With this consideration, a single-stage for spectral broadening and contrast enhancement may prove to be beneficial for the overall stability and operation of the ultrashort seed source of a petawatt-class laser.

In addition to contrast enhancement, XPW generates shorter pulses arising from (1) the cubic intensity dependence of the process (pulse shortening by $\sqrt{3}$) and (2) the interplay of SPM and cross-phase modulation (XPM) between the input laser pulse and XPW pulse. Pulse shortening above this $\sqrt{3}$ factor has been validated in several single-crystal XPW setups with the key feature of having an excellent incident beam profile on the crystal, permitting the attainment of high intensities and avoiding self-focusing within the crystal. The

smooth beam profiles were either provided by a fiber-based laser [15] or obtained in Ti:Sa systems with spatial filters in the forms of a pinhole [16] and short hollow waveguide [17]. In this paper, we present a single-stage, 10-fs, high-contrast seed source based solely on cross polarized wave generation. The fundamental aim of this work is to design and demonstrate a novel setup in order to simplify and assure robustness of XPW for long term operation, appropriate for seeding a high energy laser chain. As spectral broadening via XPW requires working at intensities near the supercontinuum generation limit ($\sim 10^{12}$ W/cm^2), the main bottleneck is related to crystal darkening and damage. Our configuration is based on a dual-crystal setup, optimized to allow spectral broadening to reach the 10-fs regime but operating below the supercontinuum generation limit ($<10^{12}$ W/cm^2) to avoid crystal darkening. Simulations are performed to determine the safe operation points on both crystals and experimental results are discussed. The final configuration also takes the reliability of the system into consideration and thus a straightforward and very compact dual-crystal XPW setup is suggested. With a minimum number of elements, it only includes the two crystals which act as windows for the vacuum chamber, a hollow waveguide for spatial filtering, a focusing mirror, and a polarizer. This ultrashort seed source has been validated to support 10-fs pulses and has an estimated temporal contrast of at least 10^{10}. It will serve as the ultrashort seed source for the Apollon 10PW project, a hybrid OPCPA-Ti:Sa laser chain being developed in France with the goal of generating 10-PW pulses.

2. SIMULATION OF SINGLE-CRYSTAL XPW PULSE SHORTENING

Temporal pulse shortening arises from XPW because it is a third order nonlinear effect, leading to a cubic dependence of the XPW intensity on the input laser intensity. A Fourier transform limited input pulse will undergo temporal pulse shortening by a factor of $\sqrt{3}$ owing to this cubic intensity dependence. Moreover, provided that the laser intensity incident on the crystal is high enough, spectral broadening greater than the $\sqrt{3}$ factor is achievable. Several nonlinear effects take place simultaneously in the crystal as given by the system of equations describing the process [18]

$$-i\frac{dA}{d\xi} = \gamma_1|A|^2A + 2\gamma_3|B|^2A + \gamma_4|B|^2B + \gamma_2AAB^* + 2\gamma_2|A|^2B + \gamma_3BBA^*, \quad (1)$$

$$-i\frac{dB}{d\xi} = \gamma_5|B|^2B + 2\gamma_3|A|^2B + \gamma_2|A|^2A + \gamma_4BBA^* + 2\gamma_4A|B|^2 + \gamma_3AAB^*, \quad (2)$$

where the fundamental input and XPW waves are designated by A and B, respectively. The first term of both equations represent the contribution of SPM, the second terms are for XPM, while the third terms are the contribution of XPW. At high input laser intensities, these additional processes contribute to further spectral broadening of the XPW pulse as the input laser pulse is broadened via SPM which is coupled to the XPW pulse. For holographic cut crystals [011], the gamma terms are summarized in Table 1.

Table 1. Coefficients for XPW Generation in Holographic Cut Crystals[a] [18]

γ_1	$\gamma_0[D - (\sigma/4)\cos 2\beta]$
γ_2	$-(\gamma_0\sigma/8)\sin 2\beta(3\cos 2\beta - 1)$
γ_3	$(\gamma_0/3)[D - (3\sigma/4)\cos 4\beta]$
γ_4	$(\gamma_0\sigma/8)\sin 2\beta(3\cos 2\beta + 1)$
γ_5	$\gamma_0[D + (\sigma/4)\cos 2\beta]$

[a]The term $\sigma = [\chi^{(3)}_{xxxx} - 3\chi^{(3)}_{xxyy}]/\chi^{(3)}_{xxxx}$ is the anisotropy of $\chi^{(3)}$, $\gamma_0 = 6\pi\chi^{(3)}_{xxxx}/8n\lambda$, and $D = 1 + (3\sigma/16)\cos 4\beta - 7\sigma/16$. For BaF_2, $\sigma = -1.2$ and $\chi^{(3)}_{xxxx} = 1.59 \times 10^{-22}$ m^2/V^2. The angle β is the orientation of the crystal with respect to the input polarization and is chosen to be 115.5° to maximize conversion of the input laser into the XPW wave.

Higher input intensities will cause larger spectral broadening but the maximum peak intensity is estimated to be around 1.5×10^{12} W/cm^2, the threshold we observed for supercontinuum generation in BaF_2. The target of the Apollon 10PW seed source is to have pulses with a bandwidth supporting 10-fs pulses. We therefore perform simulations to determine the required intensity by numerically solving Eqs. (1) and (2), including dispersion terms up to the third order, using the split-step Fourier method. Two cases are compared: a single-crystal setup pushing the intensity to the supercontinuum limit and a dual-crystal setup utilizing lower intensities.

The reference case is a single-crystal experimental setup consisting of an input laser having 25-fs and 1.5-mJ pulses from a multipass Ti:Sa amplifier (Femtolasers), as shown in Fig. 1. The pulses are then focused by a 1.5-m concave mirror within a vacuum chamber containing a 2.5-mm BaF_2 crystal and is sealed with two 500-μm thick fused silica windows. To have a smooth beam profile on the crystal, a short hollow waveguide spatially filters the input laser beam. This significant part of the setup removes any hot spots in the incident spatial profile, reaching intensities near the supercontinuum limit of the crystal and avoiding self-focusing [17]. The remaining energy on the crystal is 1.15 mJ and the beam size is 2 mm, for an intensity of around 1.5×10^{12} W/cm^2, to access enough nonlinear effects in the crystal. The XPW wave is efficiently generated in the holographic cut crystal and is separated from the input laser beam with a thin film polarizer having an extinction ratio of 10^2. This single-crystal configuration is capable of strong pulse shortening from 25-fs pulses down to the 10-fs range with a conversion efficiency of 30%. The spectrum of the pulses supports a Fourier-transform-limited (FTL) duration of 8.4 fs and experimentally, the pulses were compressed with chirped mirrors down to 9.6 fs [17].

The previous experimental results are studied further with the aid of simulations. Input conditions of the simulation are chosen to finely match the experiment, with main emphasis on the input laser spectrum. Similar to the output of the Ti:Sa amplifier, the incident laser pulse, A, has a super-Gaussian spectrum with a FWHM bandwidth of 60 nm. The spectral phase of the pulse can be varied, owing to the acousto-optic programmable dispersive filter (Dazzler) within the Ti:Sa amplifier and is chosen to match the experimental results. The XPW pulse B is initialized to zero. The crystal length is set to 2.5 mm and the input intensity is scanned up to 1.5×10^{12} W/cm^2.

In the interest of generating shorter pulses, the FTL temporal duration of the fundamental beam and XPW pulses are plotted in Fig. 2(a) with respect to the input laser intensity. The two broadening mechanisms which occur in the XPW

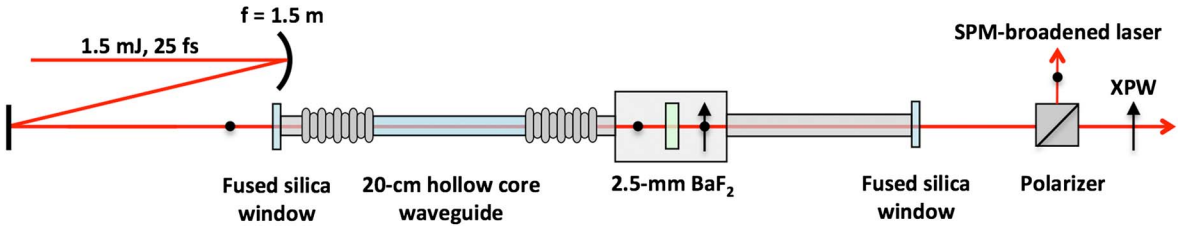

Fig. 1. Single-crystal XPW setup for spectral broadening. The vacuum chamber is sealed with two fused silica windows. XPW generation occurs within the 2.5-mm BaF_2 crystal as indicated by the dot and arrow symbols for polarization.

crystal are clearly evident in Fig. 2(a). The FTL pulse duration indicates that for low intensities, the main cause of spectral broadening/temporal shortening is the cubic dependence of XPW on the input intensity but SPM also starts to play a minor role in broadening the fundamental beam. As a result, the FTL pulse duration of the XPW pulse is shorter than the fundamental beam up to $I = 0.5 \times 10^{12}$ W/cm^2. Above this intensity, SPM becomes the main broadening mechanism and the fundamental starts to support shorter pulses than the XPW beam. As the fundamental continues to broaden at higher input intensities, the XPW spectrum follows the same behavior. In general, spectral broadening exceeding the $\sqrt{3}$ factor is caused by the SPM on the fundamental which is coupled to the XPW beam via XPM, as verified in the simulation. Nevertheless, SPM on the XPW beam itself can also lead to additional broadening when it reaches a relatively high intensity that is achievable at even higher input intensities.

Another interesting feature which occurs together with the broadening process is spectral shaping, as shown in Fig. 2(b). At low intensities and up to the transition point between the

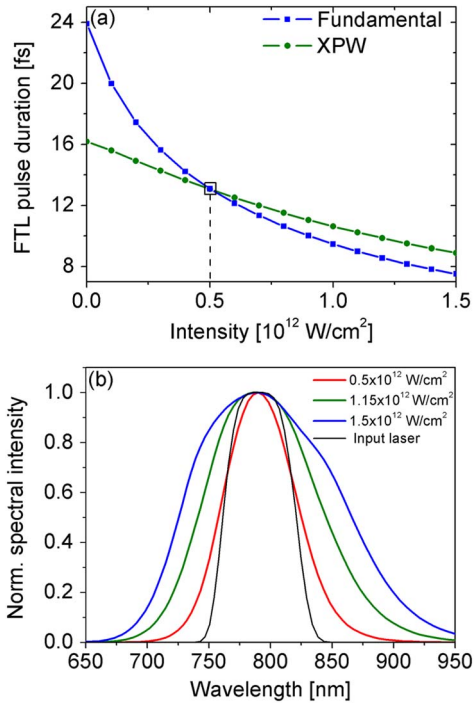

Fig. 2. (a) Temporal pulse shortening of the fundamental laser pulse (blue) and XPW pulse (green) with increasing input intensities in a 2.5-mm BaF_2 crystal. (b) Corresponding spectral broadening of the XPW spectra at input intensities of 0.5, 1.15, and 1.5×10^{12} W/cm^2 in comparison with the input laser spectrum having a FWHM of 60 nm.

broadening mechanisms of $I = 0.5 \times 10^{12}$ W/cm^2, the XPW pulse has a leptokurtic-shaped spectrum (plotted in red), with wings extending beyond the input spectrum that has a super-Gaussian shape (plotted in black). A change in kurtosis occurs at higher intensities and the spectrum is reshaped into a Gaussian-like form (plotted in green, $I = 1.15 \times 10^{12}$ W/cm^2). With an additional increase in intensity ($I = 1.5 \times 10^{12}$ W/cm^2), the spectrum broadens further and its shape approaches a higher-order Gaussian which is represented by the blue spectrum in Fig. 2(b).

The validity of the simulation is supported by the experimental results. At the experimental intensity of 1.5×10^{12} W/cm^2, 9.6 fs (8.4 fs FTL) were produced with an efficiency of 30% while in the simulation, 8.8 fs FTL pulses are obtained at the same intensity with a slightly higher efficiency of 32%. Matching the input conditions is necessary as the results with a Gaussian input spectrum overestimate the pulse shortening by SPM and XPW. Although the single-crystal setup is highly efficient [17], the required intensities to generate pulses with a spectral bandwidth supporting 10 fs appears to be too high. This led to the degradation of the crystal, eventual supercontinuum generation and the formation of a dark spot on the crystal after prolonged exposure times (typically in the week range) at a high repetition rate of 1 kHz. Possible sources of darkening are the formation of color centers in the crystal and/or impurities within the vacuum of the setup. Despite efforts to improve the vacuum, the dark spot continued to form for all BaF_2 crystal samples that have been used. Therefore, another solution to have a stable and reliable, long term operation of the ultrashort seed was imperative.

3. SIMULATION OF DUAL-CRYSTAL XPW PULSE SHORTENING

With the aim of implementing a compact and stable setup, the single-crystal setup is modified to accommodate two crystals as shown in Fig. 3. The first fused silica window of the vacuum chamber is simply replaced by a 1-mm BaF_2 crystal to create an XPW seed for the second, main XPW crystal. Since high incident intensities cause crystal degradation, the idea behind this new configuration is to perform partial conversion of the input beam into the XPW wave in the first crystal, decrease the intensity on the second crystal, yet still maintain the bandwidth to support 10-fs pulses. The XPW wave generated in the first crystal acts as a seed for the second while the fundamental beam is simultaneously spectrally broadened. The waveguide between the two crystals filters both the input and XPW beams, which removes any unwanted spatial effects created in the first crystal and provides smooth, divergent spatial profiles for XPW generation in the second crystal. Previous dual-crystal XPW setups [19] rely on the interference

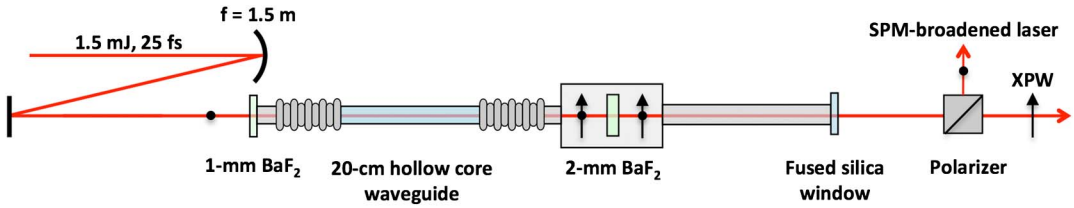

Fig. 3. Dual-crystal XPW setup for spectral broadening. After the first crystal, an XPW seed is generated thus two spatially filtered, orthogonally polarized beams (arrow and dot) are incident on the second crystal.

between the two XPW waves generated in each crystal for an efficiency improvement. However, in this new setup, seeding of the second crystal occurs with only partial conversion in the first crystal while phase matching issues between the two crystals is not crucial. In the former dual-crystal setup, the second crystal had to be positioned precisely to have interference between the generated waves in the crystals. The second crystal was typically placed out of focus to allow the accumulation of the Gouy phase. This limited the setup to low energy input pulses as the separation between the two crystals increased with respect to the available pulse energy. Simulations and experiments are performed to demonstrate the generation of 10-fs pulses with the new dual-crystal setup.

The same analysis as in the previous section is performed for the first 1-mm crystal, which generates the seed XPW pulse. This is done to determine the effect of adding the seed crystal to the incoming pulses on the main XPW crystal and for selecting an operation point for the seed crystal. The FTL pulse durations supported by the fundamental and XPW pulses are plotted in Fig. 4(a). Because of the shorter length of the crystal, the transition point between spectral broadening from XPW and SPM occurs at a higher intensity of 1.25×10^{12} W/cm^2 as indicated by the box in Fig. 4(a). An ideal operation point for the seed crystal must satisfy two conditions. The first is that it should be lower than the transition point for SPM broadening. Significant SPM in the first crystal will introduce phase shifts between the fundamental and XPW pulse that will limit the conversion efficiency in the second crystal [19]. The second condition is that the intensity should be lower than $\sim 10^{12}$ W/cm^2 to have a safe operation point. In accordance with these two conditions, $I = 0.9 \times 10^{12}$ W/cm^2 is selected for the operation point. The conversion efficiencies of the first crystal with the input intensity are shown in Fig. 4(b) and for the selected operation point, around 5.8% conversion occurs. With the insertion of the first crystal, the available spectrum for the second crystal is broadened to support 12.6 fs FTL pulses for the XPW beam and 13.4 fs FTL for the fundamental beam. Although the spectra support shorter pulses, the actual pulse durations entering the second crystal are longer due to dispersion introduced by the first crystal and the nonlinear phase contributions of XPW, SPM, and XPM. For the fundamental, the pulse lengthens to 36 fs while the XPW pulse has a duration of 20 fs and these serve as the input for the main XPW crystal. The longer pulse durations will lead to a decrease in peak intensity but the optimum intensity on the main crystal is easily chosen by adjusting beam size on second crystal. A very useful capability of the setup is the diverging output of the waveguide that permits fine-tuning of the intensity with the distance of the crystal from the end of the waveguide.

For simulating the dual-crystal setup, a simple cascade of two stages is performed. The input laser intensity of the first stage consisting of a 1-mm seed crystal, is fixed to the operation point of 0.9×10^{12} W/cm^2 while the input XPW wave is initialized to zero. The output of the first stage is used as input for the second stage, the main crystal for XPW generation which is 2 mm. Direct cascading is carried out as a consequence of the hollow waveguide filter in between the stages. Both the XPW and input laser beams do not experience strong phase shifts from self-focusing that inhibits XPW conversion because they are filtered by the waveguide. Further phase shifts are minimized by keeping SPM on the first crystal low. Efficient XPW generation occurs in the main crystal due to the spatial quality of the laser and XPW beams and the only limitation for the optimal distance between the crystals is the intensity for supercontinuum generation.

The most interesting feature of the setup would be to verify whether 10-fs pulses can be generated at lower input intensities on the main crystal as compared to the single-crystal

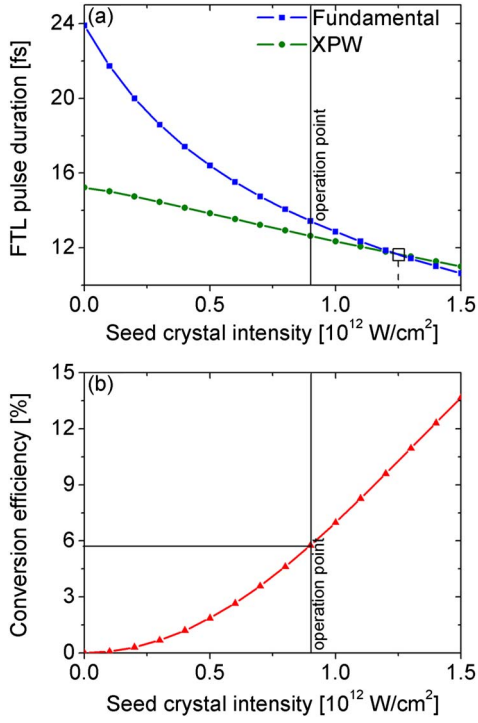

Fig. 4. Performance of the first stage (seed crystal) of the dual-crystal setup consisting of a 1-mm BaF_2 crystal. (a) FTL pulse durations supported by the broadened spectra of the fundamental (blue) and XPW pulses (green) with increasing intensities. The selected operation point for the first crystal is at $I = 0.9 \times 10^{12}$ W/cm^2. (b) Conversion efficiencies for the first stage. A 5.8% conversion efficiency is obtained at the operation point.

setup. The plots in Fig. 5(a), showing the XPW FTL pulse durations with respect to the input intensity on the main crystal, confirm that shorter pulse durations are generated at lower intensities with the dual-crystal setup than the single crystal setup. At very low input intensities ($I < 0.1 \times 10^{12}$ W/cm^2), the XPW FTL pulse duration is around 16 fs for the single-crystal setup. The result is close to the initial laser pulse duration shortened by a factor of $\sqrt{3}$ which is caused by the cubic dependence of the XPW intensity on the input laser intensity. For the dual-crystal setup, the XPW pulse in the main crystal is shorter at 12.6 fs because it is directly influenced by the XPW seed pulse and the broadened fundamental provided by the first crystal. Shorter pulses are accessible since the XPW seed pulse and the pre-broadened fundamental supply broader spectra for the XPW process as compared to the initial input laser pulse available in the single-crystal case. For both setups, the FTL pulse durations shorten almost-in-parallel with increasing intensity values and thus for the same intensity values, the dual-crystal setup always generates shorter pulses. The experimental operation point of the single-crystal setup can be matched in the simulation to yield around 8.8 fs FTL pulses at 1.5×10^{12} W/cm^2. A similar pulse duration of 8.7 fs is obtainable at a safe operation point in the dual-crystal setup at 0.9×10^{12} W/cm^2 [dashed lines in Fig. 5(a)] on the main crystal, assuring that both crystals are operating at a safe intensity below the supercontinuum generation limit. Further reduction of the intensity on the main crystal is possible with the target of obtaining 10-fs pulses. For the single-crystal setup, this pulse duration is achieved at $I = 1.15 \times 10^{12}$ W/cm^2, a value still above the safe intensity level. The input intensity is almost halved down to 0.6×10^{12} W/cm^2

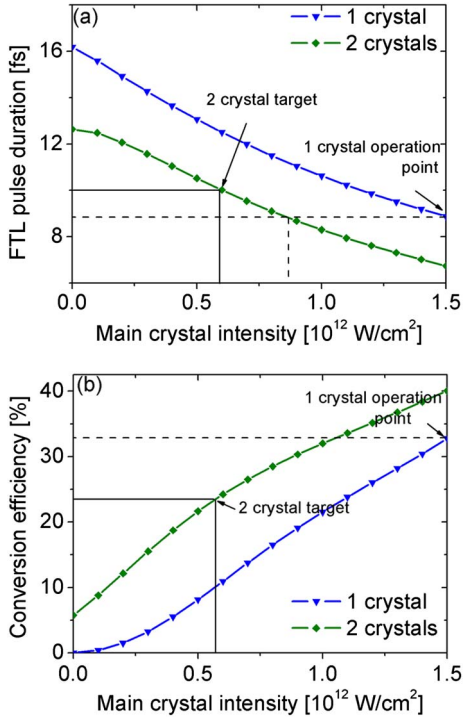

Fig. 5. Comparison between simulations for the single (blue) and dual (green) crystal XPW setups in terms of (a) FTL pulse duration of the XPW pulse and (b) conversion efficiency with respect to the input intensity on the main crystal. Dashed lines indicate the operation point of the single-crystal setup while solid lines mark the target for the dual-crystal setup.

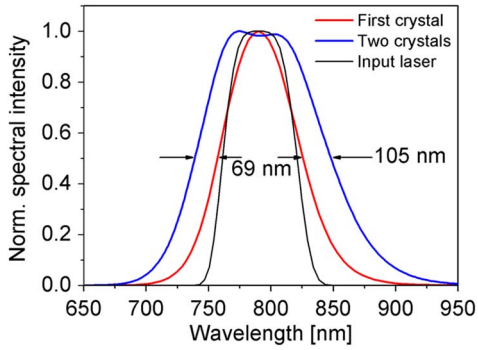

Fig. 6. Comparison of the spectrum of the input laser plotted in black (FWHM = 60 nm), the first crystal spectrum in red (FWHM = 69 nm) and dual-crystal spectrum in blue (FWHM = 105 nm).

in the dual-crystal configuration, as marked by the solid line in Fig. 5(a), to achieve 10 fs. The results ensure lower intensities on the second crystal and the avoidance of crystal darkening and supercontinuum generation. Furthermore, given that the length of the second crystal is twice as long as the first, it is essential that the intensity on the second crystal must be lower than the first to avoid self-focusing effects.

The conversion efficiency of the dual-crystal setup is also investigated and the simulation results compared to the single-crystal setup are summarized in Fig. 5(b). In general, higher conversion efficiencies are obtained with the dual-crystal setup than the single-crystal setup as a result of the total length of the crystal. The single-crystal setup has a 2.5-mm crystal whereas the dual-crystal setup has 1-mm and 2-mm crystals, for a total length of 3 mm. Long crystals are limited by the occurrence of self-focusing and SPM within the crystal but with the introduction of the hollow waveguide filter in between the two crystals, these issues are avoided in the new setup. The operation point for the single-crystal setup and the target operation point for the dual-crystal setup are indicated in Fig. 5(b) by the dashed and solid lines, respectively. In XPW, high conversion efficiencies are expected with high input intensities. With the goal of working at a lower intensity ($0.6 - 0.9 \times 10^{12}$ W/cm^2) in the dual-crystal setup, the efficiency is slightly reduced to around 24%–30% as compared to the efficiency at the operating point of the single crystal setup of around 32% ($I = 1.5 \times 10^{12}$ W/cm^2). The result is a minor trade-off in terms of the reduction of the intensity on both crystals which is expected to improve the long term operation of the whole setup.

The input laser spectrum and the XPW spectra in the first and second crystals are plotted for comparison in Fig. 6 at the target operation point of 0.6×10^{12} W/cm^2. The results also exhibit spectral shaping characteristics similar to the single-crystal setup as discussed earlier. The XPW output of the first crystal has wings broader than the input super-Gaussian spectrum, implying broadening dependent on the cubic intensity of the input. On the other hand, SPM-based broadening occurs in the second crystal as the shape approaches a higher-order Gaussian.

4. EXPERIMENTAL RESULTS WITH THE DUAL-CRYSTAL XPW SETUP

Guided by the simulation results, the dual-crystal setup was implemented as in Fig. 3, with an optimized position and

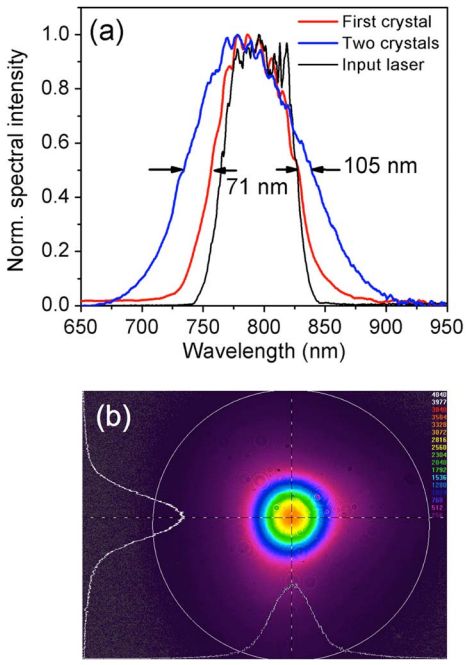

Fig. 7. (a) Similar to the simulation results the spectrum of the input laser is plotted in black (FWHM = 60 nm), the XPW output of the first crystal is indicated in red (FWHM = 71 nm) while the spectrum from the dual-crystal setup is shown in blue (FWHM = 105 nm). (b) Spatial profile of the XPW beam.

alignment of the waveguide and both crystals oriented to deliver maximum XPW conversion. The input laser had an energy of 1.2 mJ and pulse duration of 25 fs. The first crystal distance was fixed such that around 5.8% conversion occurred. The XPW output of the first crystal after transmission through the waveguide was around 42 μJ and its spectrum is shown in red in Fig. 7(a). It supports 15-fs pulses, a bit longer than the XPW seed of the simulation which was 12.6 fs. The total energy incident on the second crystal was estimated to be around 725 μJ. With the partial conversion of the input laser to the XPW seed and temporal broadening due to dispersion in the first crystal, the peak intensity on the second crystal was lowered from 1.5×10^{12} W/cm^2 to 0.64×10^{12} W/cm^2. The decrease in intensity was also visually evident, making the laser spot on the crystal less bright. Additionally, the onset of supercontinuum generation, which was previously observed for the single-crystal setup was also suppressed.

The setup in Fig. 3 was used to access the spectrum generated by the first crystal simply by removing the second crystal located in the vacuum chamber. Fine-tuning of the intensity on the second crystal was straightforward with the space provided by the vacuum chamber. This flexible configuration was initially used to determine the exact positions for both crystals. For the final setup, the crystal distances were fixed and the box-like vacuum chamber was removed. Each crystal acted as a window for the ultra-compact vacuum chamber, consisting only of the hollow core waveguide centered within metal tubes as illustrated in Fig. 8. Nonlinear effects from free propagation in air of the fundamental and XPW beams are avoided as their peak powers exiting the second crystal are below the critical power for self-focusing [20].

The performances of the test and final setups were verified to be similar. A smooth, Gaussian-like spectrum with a bandwidth of 105 nm as plotted in Fig. 7(a) was obtained, yielding an energy of 230 μJ. The shape of the spectrum from the second crystal supports the improvement of contrast of the pulse since its Fourier transform will be free of pedestals as compared to other spectral shapes such as the super-Gaussian spectral input. The similarities of the spectral shapes in the experiment corroborate the simulation results but their slight differences arise from the spectral phase present in the experiment that was difficult to precisely reproduce in the simulation. Similar to the predictions in the dual-crystal setup simulations, SPM is reduced because of the lower intensity on the second crystal but shorter pulses are still achieved via spectral broadening of the fundamental and presence of the XPW seed. The overall efficiency of the setup is 16% while the internal efficiency corresponded to 24.5%, values which are not far from the single crystal results of 20% overall and 30% internal efficiencies. The decrease in efficiency is a direct result of the lower intensity on the second crystal. Also shown in Fig. 7(b) is the excellent spatial profile of the XPW beam, ideal for injection in the succeeding parts of the laser chain.

Initially with the single-crystal setup, the crystal had to be moved laterally to expose a new point which could be used for approximately one week before a dark spot began to form. In the dual-crystal setup, this was not necessary and dark spots were never observed on the crystal during an operation period for over a year, confirming the improvement of the lifetime of the crystals and long term operation of the ultrashort seed source. Furthermore, the energy stability of the dual-crystal setup was comparable to the previous results with the single-crystal setup.

Finally, the XPW pulse was compressed with 14 reflections on chirped mirrors from Femtolasers (~ -680 fs^2) and fine dispersion control was carried out with a pair of fused silica wedges. A FROG measurement was taken to verify compression down to 10-fs pulses. The results are shown in Fig. 9 with the temporal and spectral profiles obtained from the FROG measurement. The compressed pulse had a duration of 10.7 fs, slightly longer than the target value because of the low yet non-negligible amount of uncompensated phase introduced by the chirped mirrors. Nevertheless, the XPW spectrum supported a FTL pulse duration of 9.6 fs. To facilitate compression with several reflections on chirped mirrors, a

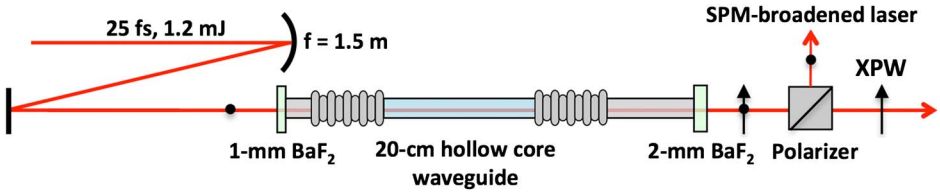

Fig. 8. Ultra-compact dual-crystal XPW setup for spectral broadening.

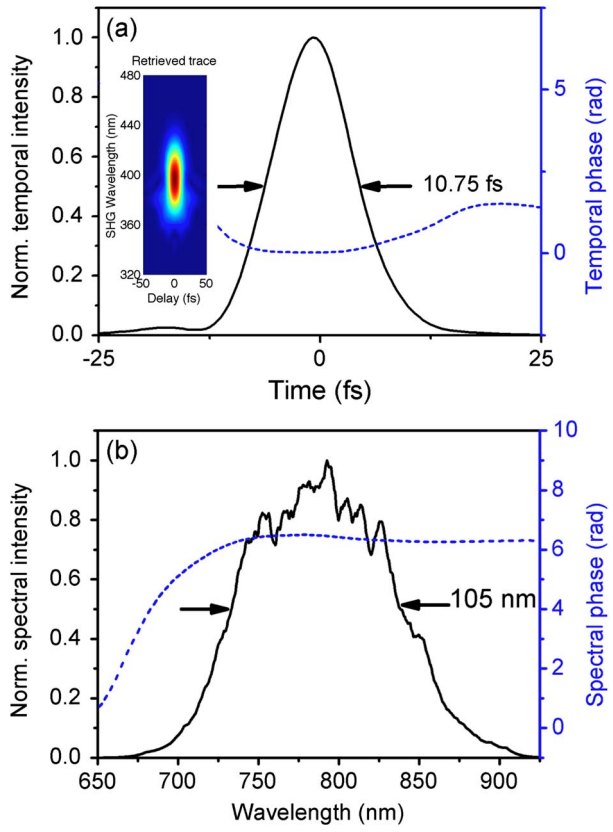

Fig. 9. (a) Temporal characterization of the two-crystal XPW pulse via FROG. Temporal profile and temporal phase with retrieved trace as inset (error = 0.18%) and (b) spectral intensity and phase of the pulse.

low dispersion, thin film polarizer was used to separate the laser and XPW pulses. The polarizer had an extinction ratio of 10^2, allowing a good estimation of the contrast enhancement from 10^8 to 10^{10} [19] as in the single-crystal setup. Given that this ultrashort seed source will serve as the injector for the Apollon 10PW laser chain, recompression at this point is not required. Therefore, a Glan polarizer with a better extinction ratio in the range of 10^4 can be used to improve the contrast further to 10^{12}.

5. CONCLUSIONS

A single nonlinear stage based on a combination of dual-crystal cross polarized wave generation and intermediate spatial filtering was demonstrated to simultaneously spectrally broaden and enhance the contrast of pulses produced by a commercial Ti:Sa amplifier. The dual-crystal setup performances were verified through simulations and experiments, to decrease the incident intensity on the BaF_2 XPW crystal. Working at lower intensities is beneficial for the lifetime of the crystals as high incident intensities were observed to cause crystal degradation. Pulse shortening from 25-fs to 10-fs pulses and contrast enhancement by at least two orders of magnitude to 10^{10} provide an excellent ultrashort seed source for petawatt-class laser systems involving OPCPA amplifiers, which typically require few-cycle injectors. The final configuration of the device has been further improved with the removal of the bulky vacuum chamber. This led to an ultra-compact and reliable setup, with the two crystals serving as windows for the tubular vacuum chamber. The footprint of the device is only 1.25 m × 0.25 m.

ACKNOWLEDGMENTS

The authors gratefully acknowledge financial support from the ILE-APOLLON 07-CPER 017-01 contract.

REFERENCES

1. Zs. Major, S. A. Trushin, I. Ahmad, M. Siebold, C. Wandt, S. Klingebiel, T.-J. Wang, J. A. Fülöp, A. Henig, S. Kruber, R. Weingartner, A. Popp, J. Osterhoff, R. Hörlein, J. Hein, V. Pervak, A. Apolonski, F. Krausz, and S. Karsch, "Basic concepts and current status of the petawatt field synthesizer—a new approach to ultrahigh field generation," Rev. Laser Eng. **37**, 431–436 (2009).
2. C. Hernandez-Gomez, S. P. Blake, O. Chekhlov, R. J. Clarke, A. M. Dunne, M. Galimberti, S. Hancock, R. Heathcote, P. Holligan, A. Lyachev, P. Matousek, I. O. Musgrave, D. Neely, P. A. Norreys, I. Ross, Y. Tang, T. B. Winstone, B. E. Wyborn, and J. Collier, "The Vulcan 10 PW project," J. Phys. Conf. Ser. **244**, 032006 (2010).
3. J.-P. Chambaret, O. Chekhlov, G. Cheriaux, J. Collier, R. Dabu, P. Dombi, A. M. Dunne, K. Ertel, P. Georges, J. Hebling, J. Hein, C. Hernandez-Gomez, C. Hooker, S. Karsch, G. Korn, F. Krausz, C. L. Blanc, Z. Major, F. Mathieu, T. Metzger, G. Mourou, P. Nickles, K. Osvay, B. Rus, W. Sandner, G. Szabó, D. Ursescu, and K. Varjú, "Extreme light infrastructure: laser architecture and major challenges," Proc. SPIE **7721**, 77211D (2010).
4. A. Dubietis, G. Jonusauskas, and A. Piskarskas, "Powerful femtosecond pulse generation by chirped and stretched pulse parametric amplification in BBO crystal," Opt. Commun. **88**, 437–440 (1992).
5. L. Veisz, "Constrast improvement of relativistic few-cycle light pulses," in *Coherence and Ultrashort Pulse Laser Emission*, F. J. Duarte, ed. (InTech, 2010).
6. A. Jullien, X. Chen, A. Ricci, J.-P. Rousseau, R. Lopez-Martens, L. P. Ramirez, D. Papadopoulos, A. Pellegrina, F. Druon, and P. Georges, "High-fidelity front-end for high-power, high temporal quality few-cycle lasers," Appl. Phys. B **102**, 769–774 (2011).
7. J. M. Mikhailova, A. Buck, A. Borot, K. Schmid, C. Sears, G. D. Tsakiris, F. Krausz, and L. Veisz, "Ultra-high-contrast few-cycle pulses for multipetawatt-class laser technology," Opt. Lett. **36**, 3145–3147 (2011).
8. I. Ahmad, S. A. Trushin, Zs. Major, C. Wandt, S. Klingebiel, V. Pervak, A. Popp, T.-J. Wang, M. Siebold, F. Krausz, and S. Karsch, "Front end light source for short-pulse pumped OPCPA System," Appl. Phys. B **97**, 529–536 (2009).
9. Y. Tang, I. N. Ross, C. Hernandez-Gomez, G. H. C. New, I. Musgrave, O. V. Chekhlov, P. Matousek, and J. L. Collier, "Optical parametric chirped-pulse amplification source suitable for seeding high-energy systems," Opt. Lett. **33**, 2386–2388 (2008).
10. M. Nisoli, S. De Silvestri, O. Svelto, R. Szipöcs, K. Ferencz, C. Spielmann, S. Sartania, and F. Krausz, "Compression of high-energy laser pulses below 5 fs," Opt. Lett. **22**, 522–524 (1997).
11. C. P. Hauri, W. Kornelis, F. W. Helbing, A. Heinrich, A. Couairon, A. Mysyrowicz, J. Biegert, and U. Keller, "Generation of intense, carrier-envelope phase-locked, few-cycle laser pulses through filamentation," Appl. Phys. B **79**, 673–677 (2004).
12. A. Jullien, O. Albert, F. Burgy, G. Hamoniaux, J.-P. Rousseau, J.-P. Chambaret, F. Augé-Rochereau, G. Chériaux, J. Etchepare, N. Minkovski, and S. M. Saltiel, "10^{-10} temporal contrast for femtosecond ultraintense lasers by cross-polarized wave generation," Opt. Lett. **30**, 920–922 (2005).
13. J. Ma, P. Yuan, Y. Wang, H. Zhu, and L. Qian, "Numerical study on pulse contrast enhancement in a short-pulse-pumped optical parametric amplifier," Opt. Commun. **285**, 4531–4536 (2012).
14. L. Gallmann, T. Pfeifer, P. M. Nagel, M. J. Abel, D. M. Neumark, and S. R. Leone, "Comparison of the filamentation and hollow-core fiber characteristics for pulse compression into the few-cycle regime," Appl. Phys. B **86**, 561–566 (2007).
15. Y. Zaouter, L. P. Ramirez, D. N. Papadopoulos, C. Hönninger, M. Hanna, F. Druon, E. Mottay, and P. Georges, "Temporal cleaning

of a high-energy fiber-based ultrafast laser using cross-polarized wave generation," Opt. Lett. **36**, 1830–1832 (2011).
16. A. Jullien, J.-P. Rousseau, B. Mercier, L. Antonucci, O. Albert, G. Chériaux, S. Kourtev, N. Minkovski, and S. M. Saltiel, "Highly efficient nonlinear filter for femtosecond pulse contrast enhancement and pulse shortening," Opt. Lett. **33**, 2353–2355 (2008).
17. L. P. Ramirez, D. N. Papadopoulos, A. Pellegrina, P. Georges, F. Druon, P. Monot, A. Ricci, A. Jullien, X. Chen, J. P. Rousseau, and R. Lopez-Martens, "Efficient cross polarized wave generation for compact, energy-scalable, ultrashort laser sources," Opt. Express **19**, 93–98 (2011).
18. L. Canova, S. Kourtev, N. Minkovski, A. Jullien, R. Lopez-Martens, O. Albert, and S. M. Saltiel, "Efficient generation of cross-polarized femtosecond pulses in crystals with holographic cut orientation," Appl. Phys. Lett. **92**, 231102 (2008).
19. A. Jullien, S. Kourtev, O. Albert, G. Chériaux, J. Etchepare, N. Minkovski, and S. M. Saltiel, "Highly efficient temporal cleaner for femtosecond pulses based on cross-polarized wave generation in a dual crystal scheme," Appl. Phys. B **84**, 409–414 (2006).
20. W. Liu and S. Chin, "Direct measurement of the critical power of femtosecond Ti:sapphire laser pulse in air," Opt. Express **13**, 5750–5755 (2005).